Control Allocation of an Unmanned Hybrid Aerial Vehicle

Lukas Spannagl, Guillaume Ducard

Accepted version of the paper : L. Spannagl, G. Ducard, "Control Allocation for an Unmanned Hybrid Aerial Vehicle," in Proceedings of the IEEE 28th Mediterranean Conference on Control and Automation (MED'2020), pp. 709 – 714, Saint Raphaël, France, September 15 – 18, 2020.
https://doi.org/10.1109/MED48518.2020.9182865

Control Allocation for an Unmanned Hybrid Aerial Vehicle

Lukas Spannagl[1] and Guillaume Ducard[2]

***Abstract*— This work presents a novel control allocation strategy for model tilt-rotor type VTOL aircraft. The aircraft considered has four tilting propellers and the aerodynamic actuators of an airplane. Control allocation converts the high-level commands in terms of total desired thrust and torques into commands distributed among the vehicle's eleven actuators. The proposed method independently tilts two pairs of propellers to generate torque along the thrust vector, which results in close-to-optimal solutions while being computationally efficient. This approach showed promising results both in simulation and tests on the vehicle and can be used in combination with any controller that generates a two-dimensional thrust and a three-dimensional torque vector.**

I. Introduction

UAVs with fixed rotors (e.g. multicopters) have vertical takeoff and landing (VTOL) capabilities, but their forward flight efficiency is low because a large amount of thrust is required to counter gravity. Fixed-wing vehicles (e.g. airplanes) on the other hand, are very efficient when it comes to forward flight, but lack the VTOL capabilities. Hybrid or convertible UAVs combine VTOL capabilities with efficient forward flight by utilizing propellers to take off vertically and wings for efficient cruising. This concept has been explored using tailsitters [1], [2], rotary wing vehicles [3], [4], [5], fixed-wing tilting-rotor aircraft [6] and others. The aircraft considered in this paper is a fixed-wing tilting-rotor type of aircraft, where the motors are mounted on top of tilting levers (Fig. 1). There is an off-the-shelf control scheme for this type of vehicle, which has a multicopter mode and a fixed-wing mode. It switches back and forth between these modes and can only be in one state at a time. The goal of this paper is to develop an energy efficient control allocation, which allows the vehicle to be in a "convertible" mode during the entire flight, with the transition between hover and forward flight being continuous as opposed to binary.
In Section II the vehicle will be described in more detail, followed by modeling of the system in Section III. The proposed control allocation is presented in Section IV. This approach is then tested both in simulation and experiments on the aircraft in Section V before a conclusion is drawn (Section VI).

II. Vehicle description

The VTOL aircraft considered in this paper is shown in Fig. 1. It has a wingspan of $2\,\mathrm{m}$, a mass of $2.7\,\mathrm{kg}$, the aerodynamic actuators of a standard aircraft (ailerons, rudders and an elevator) and four propellers, which can be tilted in pairs (① with ② and ③ with ④ as defined in Fig. 1). The tilt angle of ① and ② (χ_R) can be controlled independently of the tilt angle of ③ and ④ (χ_L). Fig. 2 shows how the tilt angle is defined. Propellers ① and ③ rotate clockwise and propellers ② and ④ rotate counter-clockwise. The aerodynamic surfaces have a maximum deflection of $\pm 35\,\mathrm{deg}$ and the tilt mechanism has a range of $-7\,\mathrm{deg}$ to $90\,\mathrm{deg}$. The two sides of the tilting mechanism can be tilted independently. By tilting the two pairs of propellers in different directions, a torque in the x-z-plane can be generated. This way of generating torque (differential tilt) can be used in addition to how a conventional drone generates torque (differential thrust). The aircraft is controlled using a 3DR Pixhawk 1 flight controller with a $168\,\mathrm{MHz}$ processor and $1\,\mathrm{MB}$ of flash memory. These hardware specifications require the control allocation to be efficient, both in terms of required processing power and memory. For state estimation [7] the vehicle has a gyroscope, an accelerometer, a magnetometer, a barometer, a pitot tube and a GPS antenna. Additionally, an antenna for telemetry data and one for the remote controller (RC) are built in. The aircraft has five actuators that control ailerons, rudders and elevator and two more servos to tilt the propellers. These seven servos in addition to four motors give the control allocation 11 degrees of freedom (DoF).

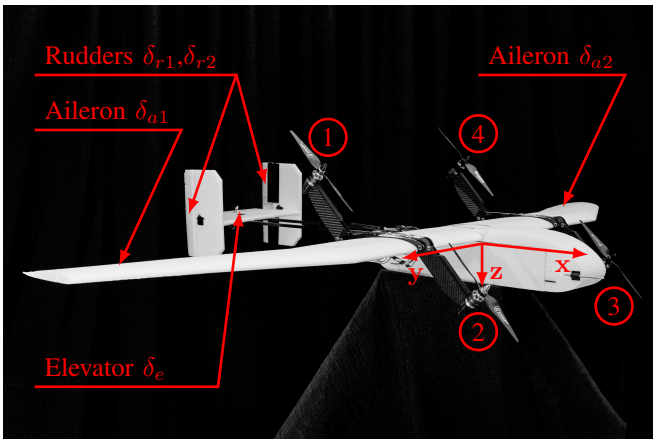

Fig. 1. Image of the considered vehicle with four propellers, two tilting mechanisms, two rudders, one elevator and two ailerons. The propellers are numbered as indicated by the circled numbers and the North-East-Down (NED) body frame is shown.

III. Forces and Torques Model

A model, which describes the effect of the actuators on the vehicle dynamics is required for the control allocation. This section is based on [8].

[1]Lukas Spannagl is with the Institute for Dynamic Systems and Control, ETH Zurich, Switzerland (e-mail:spalukas@ethz.ch).
[2]Guillaume Ducard is with I3S, University Cote d'Azur, CNRS, Sophia Antipolis, France (e-mail: ducard@i3s.unice.fr).

A. Forces

The force vectors $\mathbf{T}_i$ ($i = 1 \dots 4$) of the propellers in a North-East-Down (NED) body frame are as follows:

$$\mathbf{T}_i = -t_i \cdot R_{\chi,R/L} \cdot \mathbf{e}_3 = -t_i \cdot \begin{pmatrix} -\sin(\chi_{R/L}) \\ 0 \\ \cos(\chi_{R/L}) \end{pmatrix}, \quad (1)$$

where t_i is the scalar thrust generated by the i-th propeller, $R_{\chi,R/L}$ are the rotation matrices used to rotate the thrust according to the tilt angle $\chi_{R/L}$ and $\mathbf{e}_3$ is the body frame's z-axis. The resulting total thrust $\mathbf{T}$ is

$$\mathbf{T} = \sum_i \mathbf{T}_i \,. \quad (2)$$

B. Moments

Moments arise from the propellers (drag and thrust) and from the aerodynamic surfaces. The total rotor moment M_r is modeled as

$$\mathbf{M}_r = \sum_i \left[\lambda_i \cdot \frac{C_Q}{C_T} \cdot \mathbf{T}_i + d_{ri} \times \mathbf{T}_i \right] . \quad (3)$$

with $\lambda_1 = \lambda_3 = 1$ (clockwise rotation), $\lambda_2 = \lambda_4 = -1$ (counter-clockwise rotation), C_Q and C_T describing the resisting torque and the thrust coefficients of the propellers, respectively, and both being parameters that depend on the propeller geometry. The lever arms $d_{ri} = d_i + R_{\chi,R/L} \cdot d_{ei}$ consist of a constant term (d_i) and one that depends on the tilt angle of the arm ($R_{\chi,R/L} \cdot d_{ei}$), with

$$\begin{aligned} d_1 &= [-l_3 \quad L_0 \quad -h_0]^T, & d_{e1} &= [-l_1 \; 0 \; -h_1]^T \\ d_2 &= [\; l_4 \quad L_0 \quad -h_0]^T, & d_{e2} &= [\; l_1 \; 0 \; -h_1]^T \\ d_3 &= [\; l_4 \quad -L_0 \quad -h_0]^T, & d_{e3} &= [\; l_1 \; 0 \; -h_1]^T \\ d_4 &= [-l_3 \quad -L_0 \quad -h_0]^T, & d_{e4} &= [-l_1 \; 0 \; -h_1]^T \end{aligned}$$

Here, L_0 is defined as the distance in the y-direction from the center of gravity (CoG) to the tilting plane of one of the arms, with the rest of the dimensions being defined in Fig. 2. The aerodynamic moments in the body frame are modeled as

$$\mathbf{M}_a = \begin{pmatrix} \bar{q} \cdot S \cdot b \cdot C_{L,a} \cdot \delta_a \\ \bar{q} \cdot S \cdot \bar{c} \cdot C_{M,e} \cdot \delta_e \\ \bar{q} \cdot S \cdot b \cdot C_{N,r} \cdot \delta_r \end{pmatrix}, \quad (4)$$

where $\bar{q}$ is the dynamic pressure, S is the area of the main wing, $\bar{c}$ is the mean chord length of the main wing, b is the wingspan, C_i are coefficients that depend on the geometry of the aerodynamic actuators and δ_j ($j = a, e, r$) are the deflections of the ailerons, elevator and rudders. The total moment $\mathbf{M}$ due to actuators:

$$\mathbf{M} = \mathbf{M}_r + \mathbf{M}_a \,. \quad (5)$$

IV. Control Allocation

The aircraft has a total of eleven actuators. The goal of the control allocation is to map the desired thrust in the body x- and z-direction (T_x, T_z) and the roll/pitch/yaw moments (L, M, N) to the eleven actuators. A thrust in the y-direction cannot be realized due to the geometry of the vehicle (see Section III). The eleven actuators can be reduced to nine degrees of freedom (DoF) by making the following two assumptions:

- The two rudders are operated in parallel ($\delta_{r1} = \delta_{r2} = \delta_r$)
- The two ailerons are operated with the same magnitude, but opposite sign ($\delta_{a1} = -\delta_{a2} = \delta_a$)

Therefore, the objective is to determine the actuator-state vector $\mathbf{S} = [t_1, t_2, t_3, t_4, \chi_L, \chi_R, \delta_a, \delta_e, \delta_r]^T$, given $\mathbf{FM} = [T_{x,des}, T_{z,des}, L_{des}, M_{des}, N_{des}]^T$.

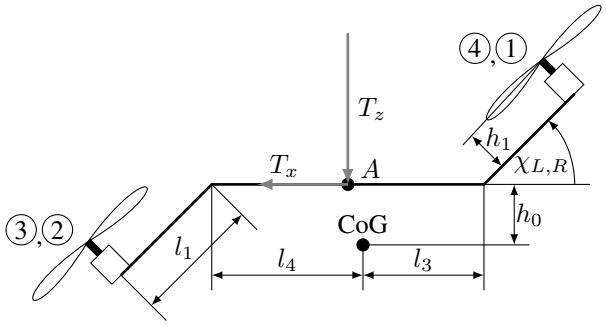

Fig. 2. Side view of the (left, right) tilt mechanism with a tilt angle of $\chi_{L,R} = \pi/4$

A. Algorithm

The goal of the control allocation is to find an actuator-state vector that results in the torques and forces given by $\mathbf{FM}$ and requires as little energy as possible. This could be solved as a constrained optimization problem. However, the Pixhawk's computing power is not sufficient to solve the optimization online at the required speed. Therefore, the following algorithm was implemented, which performs similarly well, as can be seen in Section V-A. The elements of the actuator-state vector are computed in the following order:

1) Aerodynamic Actuator States $\delta_a, \delta_e, \delta_r$
2) Tilt Angles χ_L, χ_R
3) Thrusts t_1, t_2, t_3, t_4

This approach uses daisy chaining [9] to first realize as much of the desired torque as possible with the aerodynamic surfaces. It then utilizes the tilt mechanism to generate the residual torque and the desired thrust. This minimizes energy on the assumption that the servos require a negligible amount of energy compared to the electric motors that drive the propellers. Then, the tilt angles are computed and used to obtain a linear relationship between the elements in $\mathbf{FM}$ and the thrusts t_i. In the last step, the linear system of equations is solved to obtain the individual propeller thrust t_i ($i = 1 \dots 4$).

1) Aerodynamic Actuator States: The relationship between the deflection angles of the aerodynamic actuators and the resulting torques is given by Equation 4. However, Fig. 2 shows that the center of gravity of the aircraft does not coincide with the center of the tilt mechanism, which creates

an additional pitch torque. To apply the correct counter torque, the deflections are computed as follows:

$$\delta_a = L_{des}/(C_{La} \cdot S \cdot b \cdot \bar{q}) \tag{6}$$

$$\delta_e = (M_{des} - \frac{l_3 - l_4}{2} \cdot T_z + h_0 \cdot T_x)/(C_{Me} \cdot S \cdot \bar{c} \cdot \bar{q}) \tag{7}$$

$$\delta_r = N_{des}/(C_{Nr} \cdot S \cdot b \cdot \bar{q}) \tag{8}$$

Near hover, the constant of proportionality between the desired torque and the corresponding deflection δ_j ($j = a, e, r$) becomes very large because $\bar{q} = 0.5 \cdot \rho_{air} \cdot v_{air}^2$ tends towards zero. Here, ρ_{air} is the density of air and v_{air} is the airspeed. To avoid a bang-bang control type of behavior, the deflections are multiplied with a saturated ramp function $f_1(\bar{q})$, which is linear in $\bar{q}$, zero near hover and one for large airspeeds.

$$f_1(\bar{q}) = \min(\max(0, a_{r1} \cdot (\bar{q} - b_{r1}) + 0.5), 1) \tag{9}$$

The ramp function parameters a_{rk} and b_{rk} ($k = 1, 2$) were determined in simulation to result in the desired behavior and can be found in Table I. Next, they are saturated to their maximum deflection ($\pm 35\,\mathrm{deg}$ for this vehicle) and the torques that are produced with the current airspeed and the resulting control surface deflection δ_js are subtracted from the desired torque vector to obtain a residual desired torque vector.

$$L_{des,r} = L_{des} - C_{La} \cdot S \cdot b \cdot \bar{q} \cdot \delta_a \tag{10}$$

$$M_{des,r} = M_{des} - C_{Me} \cdot S \cdot \bar{c} \cdot \bar{q} \cdot \delta_e \tag{11}$$

$$N_{des,r} = N_{des} - C_{Nr} \cdot S \cdot b \cdot \bar{q} \cdot \delta_r \tag{12}$$

2) Tilt Angles: The tilt of the propellers is computed next. The key idea here is to generate the desired torque along the direction of thrust and the thrust with a symmetric differential tilt around the direction of thrust. The mean tilt angle $\bar{\chi}$ is computed as

$$\bar{\chi} = \arctan\left(\frac{T_{x,des}}{-T_{z,des}}\right). \tag{13}$$

The residual desired torque $\boldsymbol{\tau}_{des,r} = [L_{des,r}\ M_{des,r}\ N_{des,r}]^\top$ is then projected onto the desired thrust $\mathbf{T}_{des} = [T_{x,des}\ 0\ T_{z,des}]^\top$ to obtain the magnitude of the torque along the thrust.

$$\tau_{proj} = \boldsymbol{\tau}_{des,r} \cdot \frac{\mathbf{T}_{des}}{||\mathbf{T}_{des}||} \tag{14}$$

Now, the differential tilt angle $\Delta\chi$ can be calculated as

$$\Delta\chi = \arctan\left(\frac{\tau_{proj} \cdot f_2(||\mathbf{T}_{des}||)}{||\mathbf{T}_{des}|| \cdot L_0}\right), \tag{15}$$

where L_0 is the normal distance between the CoG and one of the tilting planes. A second ramp $f_2(||\mathbf{T}_{des}||)$ is introduced to limit the amount of differential tilt when the desired thrust is low. This ensures a clean multicopter-like takeoff without tilting while still on the ground. The ramp is defined as

$$f_2(||\mathbf{T}_{des}||) = \min(\max(0, a_{r2} \cdot (||\mathbf{T}_{des}|| - b_{r2})), 1). \tag{16}$$

To obtain χ_L and χ_R we calculate

$$\chi_L = \bar{\chi} - \Delta\chi, \tag{17}$$

$$\chi_R = \bar{\chi} + \Delta\chi. \tag{18}$$

These values might not be within the valid range of the tilting mechanism (-7 to $90\,\mathrm{deg}$ for this vehicle). This has to be checked and corrected by reducing $\Delta\chi$ to the point where neither of the tilt angles is out of bounds. Note that $\bar{\chi}$ is always in the range $[0, 90]\mathrm{deg}$ because T_x is strictly positive and T_z is strictly negative.

3) Thrusts: To calculate the individual propeller thrusts t_i, the five equations resulting from equating Equation 2 with the desired thrust and Equation 5 with the desired torque are used. Note that this results in five equations because the thrust in the y direction is zero. This nonlinear system of equations becomes linear by inserting the previously calculated tilt angles χ_L and χ_R. Since the mean tilt points towards the desired thrust, solving four (three torque and one thrust equation) of the five equations is sufficient to approximately solve all five. This is a good approximation for small $\Delta\chi$ and exact for $\Delta\chi = 0$ or $t_1 + t_2 = t_3 + t_4$. Simulation and experiments on the real vehicle show that $\Delta\chi$ stays within $\pm 7\,\mathrm{deg}$. The linear system of equations is

$$\begin{pmatrix} T_x \\ T_z \\ L_{des,r} \\ M_{des,r} \\ N_{des,r} \end{pmatrix} = \begin{pmatrix} \\ \mathbf{A} \\ \\ \end{pmatrix} \begin{pmatrix} t_1 \\ t_2 \\ t_3 \\ t_4 \end{pmatrix}, \tag{19}$$

with

$$A = \begin{pmatrix} \sin(\chi_R) & \sin(\chi_R) \\ -\cos(\chi_R) & -\cos(\chi_R) \\ -L_0\cos(\chi_R) + \frac{C_Q}{C_T}\sin(\chi_R) & -L_0\cos(\chi_R) - \frac{C_Q}{C_T}\sin(\chi_R) \\ -l_1 - l_3\cos(\chi_R) - h_0\sin(\chi_R) & l_1 + l_4\cos(\chi_R) - h_0\sin(\chi_R) \\ -L_0\sin(\chi_R) - \frac{C_Q}{C_T}\cos(\chi_R) & -L_0\sin(\chi_R) + \frac{C_Q}{C_T}\cos(\chi_R) \\ \sin(\chi_L) & \sin(\chi_L) \\ -\cos(\chi_L) & -\cos(\chi_L) \\ L_0\cos(\chi_L) + \frac{C_Q}{C_T}\sin(\chi_L) & L_0\cos(\chi_L) - \frac{C_Q}{C_T}\sin(\chi_L) \\ l_1 + l_4\cos(\chi_L) - h_0\sin(\chi_L) & -l_1 - l_3\cos(\chi_L) - h_0\sin(\chi_L) \\ L_0\sin(\chi_L) - \frac{C_Q}{C_T}\cos(\chi_L) & L_0\sin(\chi_L) + \frac{C_Q}{C_T}\cos(\chi_L) \end{pmatrix}.$$

To obtain the t_is, lines $2-5$ of Equation 19 are solved if $\bar{\chi} < \pi/4$, and lines $1, 3-5$ are solved if $\bar{\chi} \geq \pi/4$. Alternatively, it would be possible to use a pseudo inverse, but this only improves the accuracy very slightly and requires more memory and computational power.

V. Simulation and Experimental Results

To test the algorithm described above, it was first implemented in Matlab, where its results were compared to the optimal actuator-state vector $\mathbf{S}$. Then, a custom Pixhawk firmware was created, which was tested using a Software in the Loop (SITL) simulation. Finally, the firmware was uploaded to the Pixhawk for experiments on the vehicle.

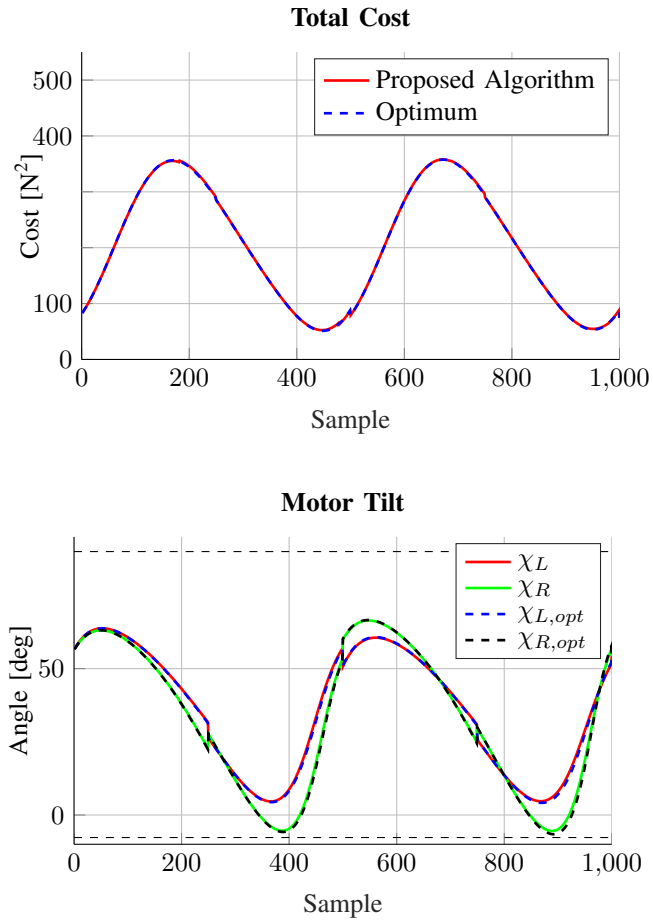

Fig. 3. This figure compares the results of the proposed algorithm with the optimal solution in terms of cost (top) and tilt angles (bottom). The graphs show how they compare for 1000 different sample-**FM**s.

A. Comparison to Optimality in Simulation

The control allocation problem can be interpreted as a constrained minimization problem. The constraints are the model described in Section III, and the cost function is defined as

$$J = \sum_i t_i^2 \,. \tag{20}$$

Minimizing this function minimizes the energy consumption on the assumption that the energy required by the servos is negligible compared to the one required by the motors. This constrained optimization problem is used to benchmark the proposed algorithm, and its output is optimal given the assumptions. The aerodynamic actuators can be decoupled from the rest of the problem because the δ_js and their derivatives do not generate cost. Therefore, the aerodynamic actuator output states, as computed in the proposed algorithm, are optimal. By setting the airspeed for this comparison to zero (= deactivating the aerodynamic actuators), only potentially non-optimal aspects of the algorithm are compared to optimality. For this comparison, 1000 different high-level command vectors **FM**s are generated and given to the proposed algorithm. The results are compared to the solution of the constrained minimization, which was obtained using FORCES PRO [10] [11]. In Fig. 3, the total cost and the tilt angles are compared. This comparison in simulation shows that the proposed algorithm gives close-to-optimal results, both in terms of tilt angle and total cost.

B. With and Without Differential Tilt

To simulate the effect for differential tilt, the algorithm described in Section IV-A was implemented in a custom Pixhawk firmware, which also contains the FPID controller described in [12] to stabilize the aircraft. This firmware and vehicle were then simulated using a Gazebo SITL simulation. Within this simulation environment, the authority along the thrust vector with and without differential tilt is compared. The results for this comparison case can be seen in Fig. 4 and 5. In both scenarios, the aerodynamic actuators are inactive because the tests are conducted near hover ($\bar{q} \approx 0$) and first, at $\sim$0.4 s, a positive yaw torque is commanded followed by a negative one approximately two seconds later. For the first test, $\Delta\chi$ was manually set to zero ($\chi_L = \chi_R = \bar{\chi}$). In this case, the control allocation can only generate the desired torque using differential thrust (Fig. 4). This saturates the motors, which starts to destabilize the aircraft during the second torque command. With differential tilt (Fig. 5), the motors tilt in opposite directions and only slightly increase their thrust (by $\sim$0.4 N) to generate the desired torque. This allows to generate a larger torque with less thrust, which prevents saturation of the motors. Here, the yaw torque was considered, but the increased torque authority generalizes to any torque along the thrust vector.

TABLE I
PHYSICAL PARAMETERS OF THE AIRCRAFT

Name	Parameter	Value
Air Desity	ρ	1.2041 kg/m^3
Surface Area of Main Wing	S	0.4266 m^2
Propeller Yaw Coefficient	C_Q	$1.99017e{-}7$
Propeller Thrust Coefficient	C_T	$1.11919e{-}5$
Aileron Coefficient	C_{La}	0.11730
Elevator Coefficient	C_{Me}	0.55604
Rudder Coefficient	C_{Nr}	0.08810
Tilting plane y-Offset	L_0	0.29 m
Lever Length	l_1	0.1575 m
Position of Rear Lever Pivot	l_3	0.105 m
Position of Front Lever Pivot	l_4	0.11 m
Tilting mechanism z-Offset	h_0	0.015 m
Propeller height	h_1	0.05 m
Wingspan	b	2 m
Chord length	$\bar{c}$	0.2 m
Ramp Function 1 Slope Parameter	a_{r1}	0.0185
Ramp Function 1 Position Parameter	b_{r1}	35.217
Ramp Function 2 Slope Parameter	a_{r2}	0.25
Ramp Function 2 Position Parameter	b_{r2}	2

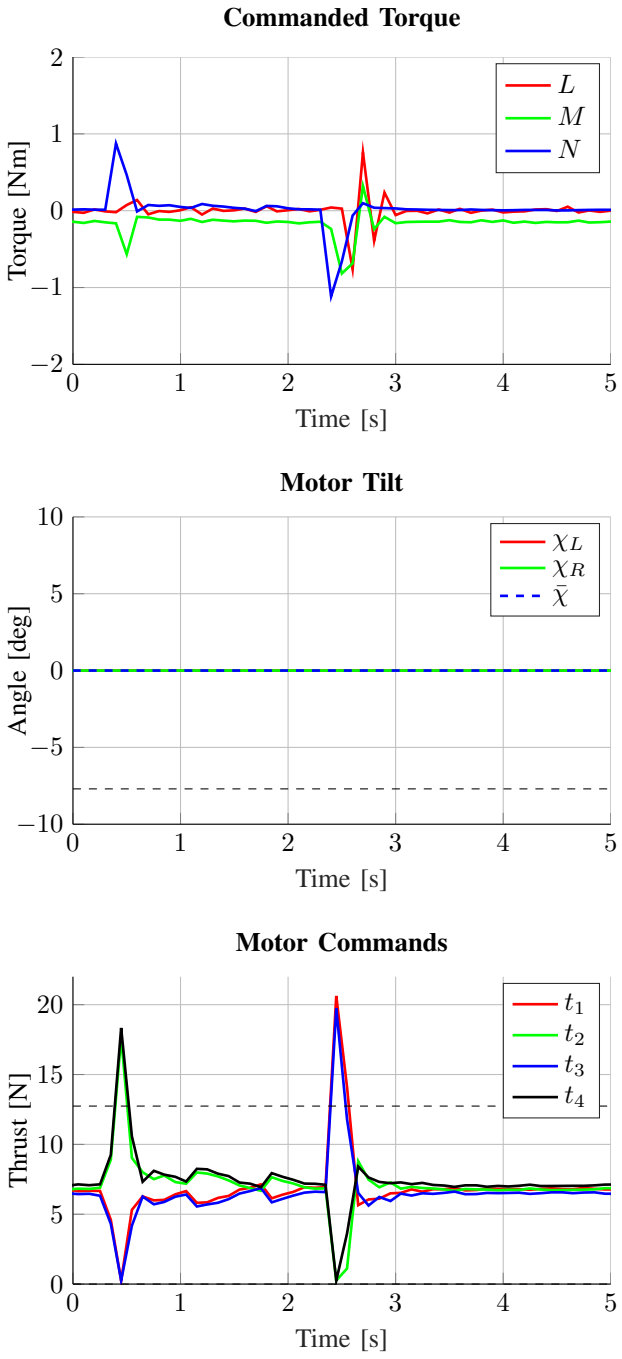

Fig. 4. This figure shows (from top to bottom) the torque commanded by the controller, the tilt angles χ_L, χ_R and $\bar{\chi}$ and the motor commands that the control allocation generates. In this case the vehicle is near hover ($\delta_a = \delta_e = \delta_r = 0$) and the differential tilt is manually disabled ($\chi_L = \chi_R = \bar{\chi}$). Dashed lines show the respective maximum values.

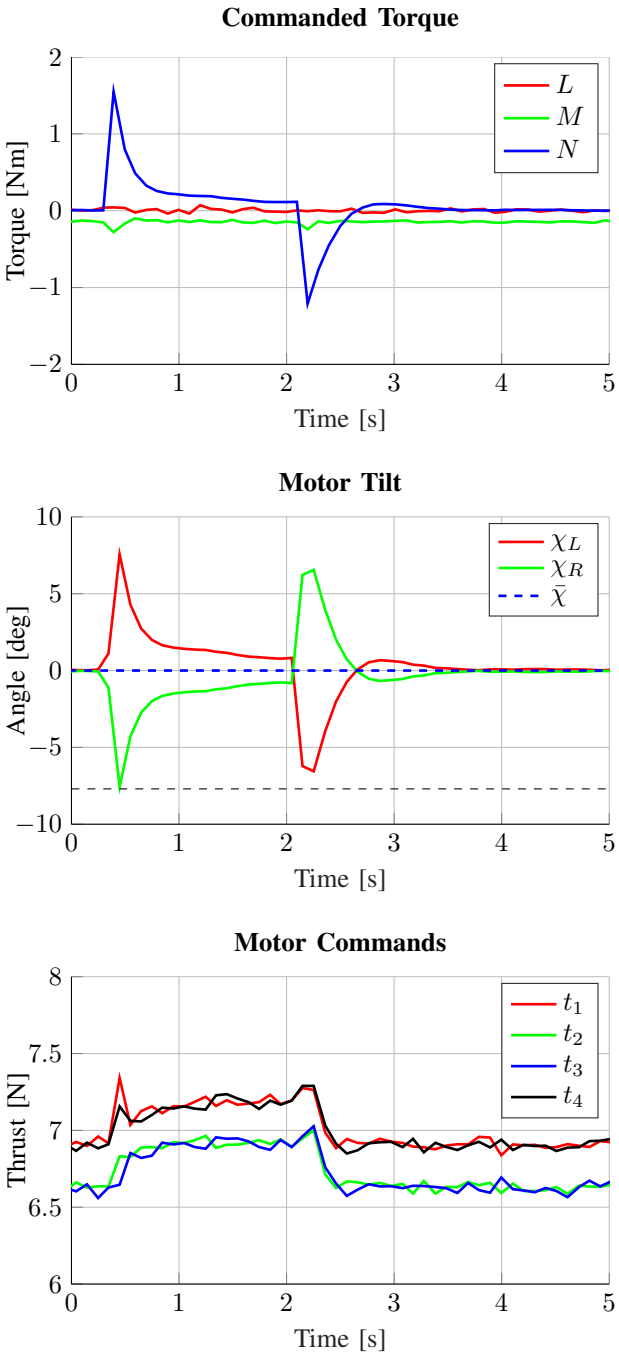

Fig. 5. This figure shows (from top to bottom) the torque commanded by the controller, the tilt angles χ_L, χ_R and $\bar{\chi}$ and the motor commands that the control allocation generates. In this case the vehicle is near hover ($\delta_a = \delta_e = \delta_r = 0$) and the differential tilt is enabled. Dashed lines show the respective maximum values.

C. Experimental results

To show the applicability of this algorithm on a real system, the firmware was uploaded to the vehicle and a flight was conducted. The results are shown in Fig. 6. In this experiment, the aircraft hovers, accelerates up to a speed of around $20\,\mathrm{m/s}$ and returns to hover. During this maneuver, the motors continuously tilt forward to about $80\,\mathrm{deg}$ and back to zero. At approximately $6\,\mathrm{s}$, the aircraft is fast enough to utilize the aerodynamic actuators and as soon as these can fully generate the commanded torque, the motors align and only generate the desired thrust (from $7.5\,\mathrm{s}$ to $16\,\mathrm{s}$). During this time, the differential tilt is also inactive, because the torque along the thrust vector is already generated by the aerodynamic actuators. The numerical values of the constants used during the experiment are shown in Table I. A video of the flight can be found at `https://youtu.be/UFTDs19QKvk`.

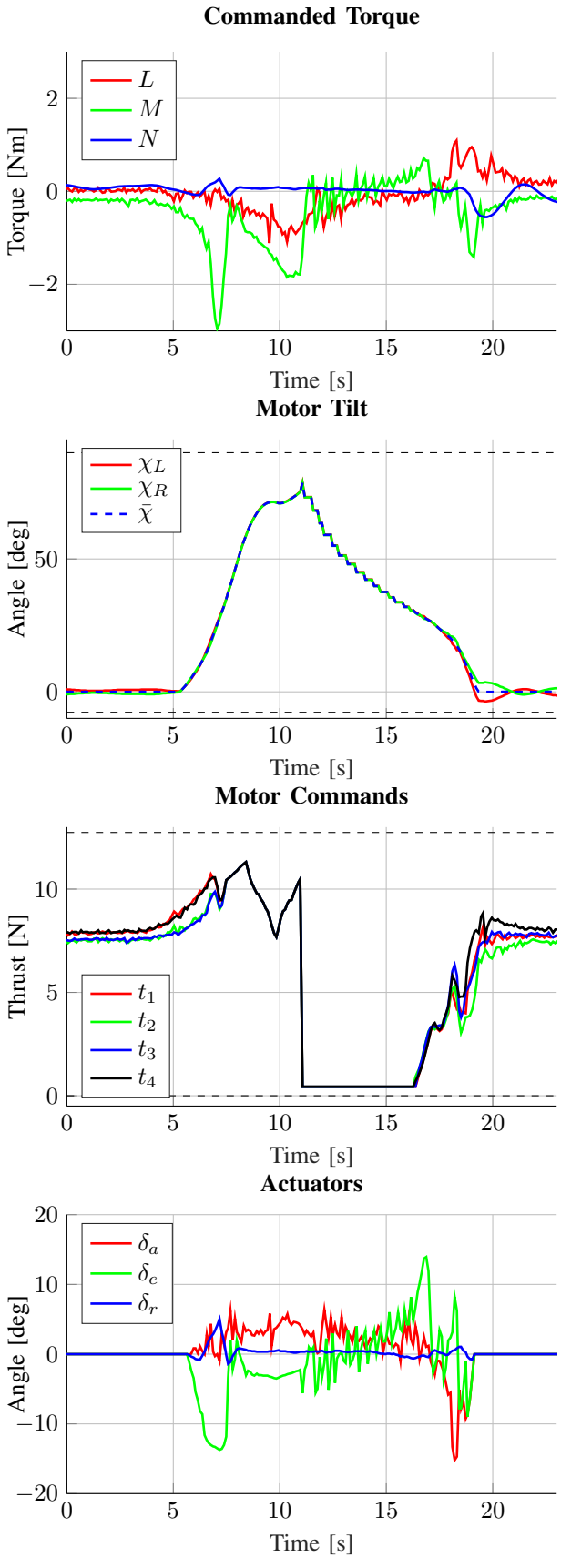

Fig. 6. This figure shows (from top to bottom) the commanded torque, the motor tilt, the motor commands and the deflections δ_j of an experiment on the vehicle.

VI. Conclusion and Outlook

This paper describes a new control allocation algorithm for tilt rotor type VTOL aircraft. This algorithm comprises three steps. First, daisy chaining is utilized to generate as much of the desired torque as possible with the aerodynamic actuators. This step is dependent on airspeed. The residual torque is then projected onto the thrust vector. This projected torque and the desired thrust result in a unique symmetric tilt angle, which is used to obtain a linear relationship between the desired high-level commands and the thrust of the individual propellers. In Step 3 of the algorithm, this linear system of equations is solved. The algorithm was validated both in simulation and on a real vehicle. The simulation showed close-to-optimal results, both in terms of tilt angle and thrust. Another simulation demonstrated superior torque authority along the thrust vector when differential tilt is enabled. Real-system tests showed that the algorithm is fast and small enough to be implemented on systems limited in processing power and memory. Furthermore, the algorithm does not show potential convergence problems, which a constrained minimization solver might have. The next steps could involve improving the hardware, such as moving the CoM as closely as possible to the center of the tilt mechanism, or designing a controller that contains information on the aircraft, e.g. a model predictive controller (MPC).

References

[1] J. Escareno, R. Stone, A. Sanchez, and R. Lozano, "Modeling and control strategy for the transition of a convertible tail-sitter UAV," in *2007 European Control Conference*. IEEE, 2007, pp. 3385–3390.

[2] D. A. Ta, I. Fantoni, and R. Lozano, "Modeling and control of a convertible mini-UAV," *IFAC Proceedings Volumes*, vol. 44, no. 1, pp. 1492–1497, 2011.

[3] E. Çetinsoy, S. Dikyar, C. Hançer, K. Oner, E. Sirimoglu, M. Unel, and M. Aksit, "Design and construction of a novel quad tilt-wing UAV," *Mechatronics*, vol. 22, no. 6, pp. 723–745, 2012.

[4] K. Muraoka, N. Okada, and D. Kubo, "Quad tilt wing vtol uav: Aerodynamic characteristics and prototype flight," in *AIAA Infotech@ Aerospace Conference and AIAA Unmanned Unlimited Conference*, 2009, p. 1834.

[5] S. Suzuki, R. Zhijia, Y. Horita, K. Nonami, G. Kimura, T. Bando, D. Hirabayashi, M. Furuya, and K. Yasuda, "Attitude control of quad rotors QTW-UAV with tilt wing mechanism," *Journal of System Design and Dynamics*, vol. 4, no. 3, pp. 416–428, 2010.

[6] G. R. Flores, J. Escareño, R. Lozano, and S. Salazar, "Quad-tilting rotor convertible mav: Modeling and real-time hover flight control," *Journal of Intelligent & Robotic Systems*, vol. 65, no. 1-4, pp. 457–471, 2012.

[7] L. Feng and Q. Fangchao, "Research on the Hardware Structure Characteristics and EKF Filtering Algorithm of the Autopilot PIXHAWK," in *2016 Sixth International Conference on Instrumentation & Measurement, Computer, Communication and Control (IMCCC)*. IEEE, 2016, pp. 228–231.

[8] G. Ducard and M. Hua, "Modeling of an unmanned hybrid aerial vehicle," in *2014 IEEE Conference on Control Applications (CCA)*, Oct 2014, pp. 1011–1016.

[9] W. S. Levine, *The control handbook: control system applications*, 2nd ed. CRC press, 2011, (chapter 8).

[10] A. Domahidi and J. Jerez, "Forces professional," Embotech AG, https://embotech.com/FORCES-Pro, 2014–2019.

[11] A. Zanelli, A. Domahidi, J. Jerez, and M. Morari, "Forces nlp: an efficient implementation of interior-point methods for multistage nonlinear nonconvex programs," *International Journal of Control*, pp. 1–17, 2017.

[12] L. Bauersfeld and G. Ducard, "Fused-PID Control for Tilt-Rotor VTOL Aircraft," 16-19 June, 2020, 28th Mediterranean Conference on Control and Automation (MED'2020) Saint-Raphaël, France.